A Synoptic Analysis of the Interannual Variability of Winter Cyclone Activity in the Aleutian Low Region

XIAOJIE ZHU

Physical Oceanography Laboratory, and Ocean–Atmosphere Interaction and Climate Laboratory, Ocean University of China, Qingdao, China, and Center for Climatic Research, University of Wisconsin—Madison, Madison, Wisconsin

JILIN SUN

Physical Oceanography Laboratory, and Ocean–Atmosphere Interaction and Climate Laboratory, Ocean University of China, Qingdao, China

ZHENGYU LIU

Center for Climatic Research, University of Wisconsin—Madison, Madison, Wisconsin

QINYU LIU

Physical Oceanography Laboratory, and Ocean–Atmosphere Interaction and Climate Laboratory, Ocean University of China, Qingdao, China

JONATHAN E. MARTIN

Department of Atmospheric and Oceanic Sciences, University of Wisconsin—Madison, Madison, Wisconsin

(Manuscript received 1 December 2005, in final form 19 May 2006)

ABSTRACT

An analysis of cyclone activity in winter associated with years of strong and weak Aleutian low in the North Pacific is presented. From 1958 to 2004, 10 winters with a strong Aleutian low are defined as the strong years, while 8 winters with a weak Aleutian low are defined as the weak years.

Employing a system-centered Lagrangian method, some characteristics of the cyclone activity in both sets of years are revealed. The cyclone frequency, duration, and intensity are nearly the same in both strong and weak years. The cyclone tracks in the strong years are more zonal than those in the weak years. More intense cyclone events and more large cyclone cases occur in strong years than in weak years and the deepening of cyclones in strong years is stronger than that in weak years. The analyses of geopotential height, wind, stationary Rossby wavenumber, and Eady growth rate index at 500 or 300 hPa reveal that conditions are favorable for more zonal tracks and greater cyclone growth in strong years than in weak years.

An estimation of the relative change of cyclone intensity and the relative change of Aleutian low intensity is made, which shows that the interannual change of cyclone intensity is about 73% of the interannual change of Aleutian low intensity. This result suggests that the evolution of individual cyclones may be a significant driver of changes in the Aleutian low.

1. Introduction

During the winter season in the North Pacific the dominant feature of the mean circulation is the Aleutian low, a semipermanent low pressure center associated with the East Asian trough in the upper troposphere. Changes in the Aleutian low have significant effects on the entire Pacific basin. The winds in the eastern and western portions of the Aleutian low center influence the heat exchange between the polar regions and the extratropical Pacific; the stronger westerlies in the southern portion of the Aleutian low may enhance the North Pacific Current, thereby spinning up the sub-

Corresponding author address: Xiaojie Zhu, Center for Climatic Research, University of Wisconsin—Madison, 1225 W. Dayton St., Madison, WI 53706-1695.
E-mail: xzhu5@wisc.edu

DOI: 10.1175/JCLI4077.1

tropical ocean gyre (Latif and Barnett 1996). Therefore, the location and intensity of the Aleutian low are among the primary indicators of the climate system in the winter North Pacific (Hartmann and Wendler 2005; Rodionov et al. 2005). Several authors have examined the interdecadal and decadal variability of the Aleutian low (Trenberth 1990; Chen et al. 1992; Trenberth and Hurrell 1994; Overland et al. 1999). From 1977 to 1988, there was a deeper and eastward-shifted Aleutian low in the winter months (December–February). With the deeper Aleutian low, warm and moist air was advected into Alaska while cold air was ushered equatorward over the central and western North Pacific (Trenberth 1990). Overland et al. (1999) investigated the intensity of the Aleutian low on the decadal scale, concentrating on the mid- and high latitudes. They found that the January–February variability of the Aleutian low is not associated solely with the Pacific–North American (PNA) pattern, but is also associated with the variability of the Arctic Oscillation. Also, the Aleutian low has a notable relationship with the Pacific decadal oscillation (PDO) as the warm (cold) phase of the PDO is associated with a deepened (weakened) Aleutian low (Mantua et al. 1997). While occurring at interannual frequencies, changes in the Aleutian low are believed to be one of the more important forcing mechanisms of the PDO (Schneider and Cornuelle 2005). Other authors have concentrated on the effect of the sea surface temperature on the intensity of the Aleutian low (e.g., Alexander 1992; Lau and Nath 1994; Latif and Barnett 1996).

There are two views of the transient wave system involved in the production and maintenance of the North Atlantic's Icelandic low. The first is that the Icelandic low is part of a background stationary planetary wave structure associated with large-scale forcing, while the second claims that the Icelandic low is the ensemble of the synoptic lows moving into the region. A similar perspective can be adopted in consideration of the Aleutian low. Wallace et al. (1988), through correlation analysis, found that cyclones developing near Japan move to the northeast and finally merge into the climatological Aleutian low. This change in the climatological system may influence subsequent cyclone activity. The location and strength of the transients are largely determined by the quasi-stationary waves, which in turn are altered by the resulting eddy energy transport (Trenberth and Stepaniak 2003). Other research on cyclone activity concentrates on regions such as the Arctic (Serreze 1995; Zhang et al. 2004), the North Pacific (Martin et al. 2001; Otkin and Martin 2004a,b), and the Icelandic low regions (Serreze et al. 1997). In this paper, we will investigate cyclone activity associated with the Aleutian low.

The first aim of the paper is to describe some of the characteristics of the cyclone activity associated with the Aleutian low. Two basic methods exist to objectively track the cyclone. The Eulerian method is based on determining statistics at a set of grid points. A map of the root-mean-square (rms) height is constructed corresponding to different spatial scales and frequency bands. The spatial scales and the frequency bands are then chosen to emphasize blocking and cyclogenesis (Blackmon 1976; Blackmon et al. 1977). The Lagrangian method is a system-centered method that identifies each individual weather system and tracks its position (Klein 1957; Gyakum et al. 1989; Anderson and Gyakum 1989; Otkin and Martin 2004a). This method is synonymous with feature tracking (Murray and Simmonds 1991a,b; Hodges 1995, 1999; Hoskins and Hodges 2002). Here, we will use a Lagrangian method to track cyclones associated with the Aleutian low, after which we will analyze some characteristics of the cyclone activity.

The second aim of this paper is to analyze the large-scale circulations within which the varying Aleutian low cyclone activity occurs. There is a close relationship between regions of large bandpass-filtered variance at the 500-hPa level and regions with a high frequency of cyclonic activity (Sawyer 1970; Lau 1988). Strong equatorward ageostrophic flow in the upper troposphere is associated with strong poleward heat flux in the lower troposphere, which may provide a favorable condition for cyclogenesis in the exit region of the jet (Blackmon et al. 1977). Considering the close relationship between cyclone activity and the large-scale circulation, it is very important to contrast the large-scale circulation patterns across the Pacific in order to better illustrate cyclone activity.

A number of studies have considered the relationship between low-frequency variability of the large-scale circulation and cyclone activity. Some of these studies have examined the effect of global warming on cyclone activity with models (Koning et al. 1993; Hall et al. 1994; Lambert 1995) or with analysis of statistical cyclone data (McCabe et al. 2001). Some others have examined the links between ENSO and weather systems and found a coherent cyclone response to ENSO (Sinclair et al. 1997). A number of studies have employed local Eliassen–Palm fluxes to diagnose dynamical interactions between the transient eddies and the mean circulation (Hoskins et al. 1983; Trenberth 1986; Lau 1988). The composite circulation at sea level and Eliassen–Palm vectors associated with various storm track modes in Lau (1988) reveal that positive Aleutian low

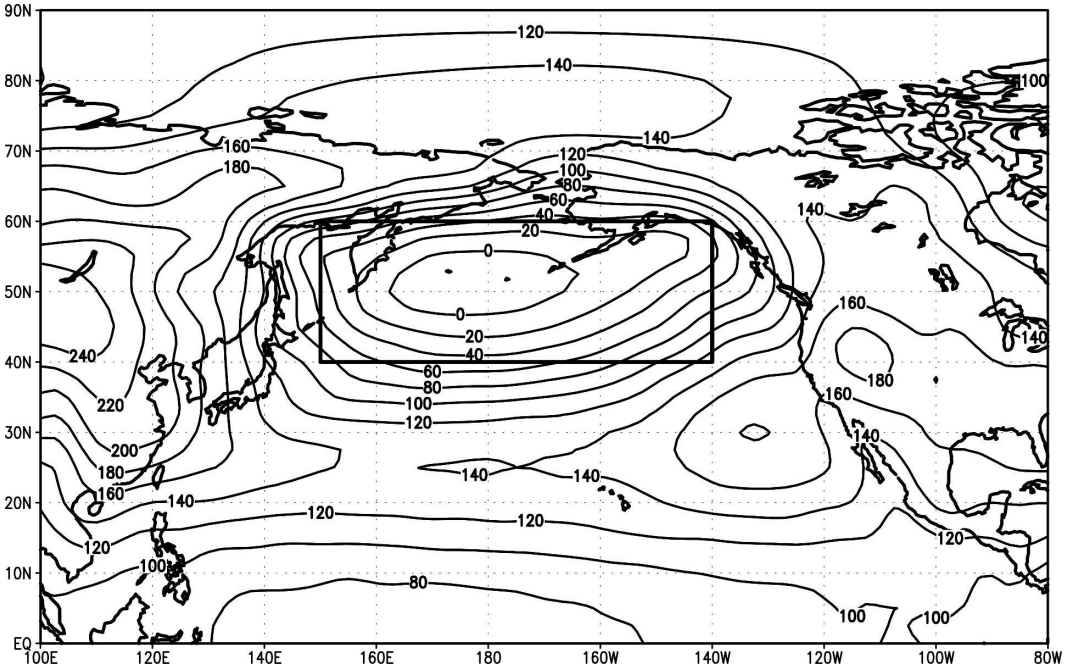

FIG. 1. Climatological 1000-hPa geopotential height field in winter [December–February (1958–2004)]. Solid lines are geopotential heights in which the counter interval (CI) is 20 gpm. The black frame is the region (40°–60°N, 150°E–140°W).

anomalies are accompanied by stronger storm tracks, while the eddy momentum transports act to accelerate the westerly mean flow along the storm track. Furthermore, the nonlinear interaction between the transient wave and the mean flow is also studied (Palmer 1998). In the present paper, in which a Lagrangian perspective is adopted, the assessment as to whether the variability of the Aleutian low is related to transient cyclone activity or represents a stationary wave response is made, not by using the Eulerian diagnostics just described, but by consideration of a conceptual mechanism that may underlie the behavior of the Aleutian low.

The paper is organized as follows: in section 2, the dataset and the analysis methods used to construct the synoptic climatology are described. The definitions of strong and weak Aleutian low years are also given in this section. The respective characteristics of the cyclone activity during strong and weak years, such as the cyclone frequency, cyclone duration, cyclone track, cyclogenesis, mature and cyclolysis stages and their respective geographical distributions, cyclone intensity, cyclone size, and the deepening of cyclone are given in section 3. In section 4, the composite large-scale circulations associated with strong and weak Aleutian lows are presented to illustrate the role of the large-scale circulations in modulating cyclone activity. A discussion about the impact of the variability of cyclone activity on the evolution of the Aleutian low is given in section 5. Finally, conclusions are presented in section 6.

2. Data and methodology

The primary data used in this paper are the National Centers for Environmental Prediction–National Center for Atmospheric Research (NCEP–NCAR) reanalysis datasets consisting of monthly and daily standard pressure level analyses on a global domain with 2.5° latitude–longitude resolution. This data ranges from January 1958 to December 2004.

Because the Aleutian low strengthens beginning in September and reaches its maximum intensity in January (not shown), the December–February time frame was selected to represent the winter. For the winter climatological 1000-hPa geopotential height field (Fig. 1), the Aleutian low is within the region 40°–60°N, 150°E–140°W, and this region was chosen to be the research area.

Within this region, the intensity and location of the Aleutian low changes with time. To better illustrate this variability, monthly data are used to show the regional averaged winter 1000-hPa geopotential height anomaly and the longitude of the minimum geopotential height (Fig. 2). Using the standard deviation as the criteria, the 1960/61, 1969/70, 1976/77, 1980/81, 1982/83, 1985/86, 1986/87, 1997/98, 2002/03, and 2003/04 winters were

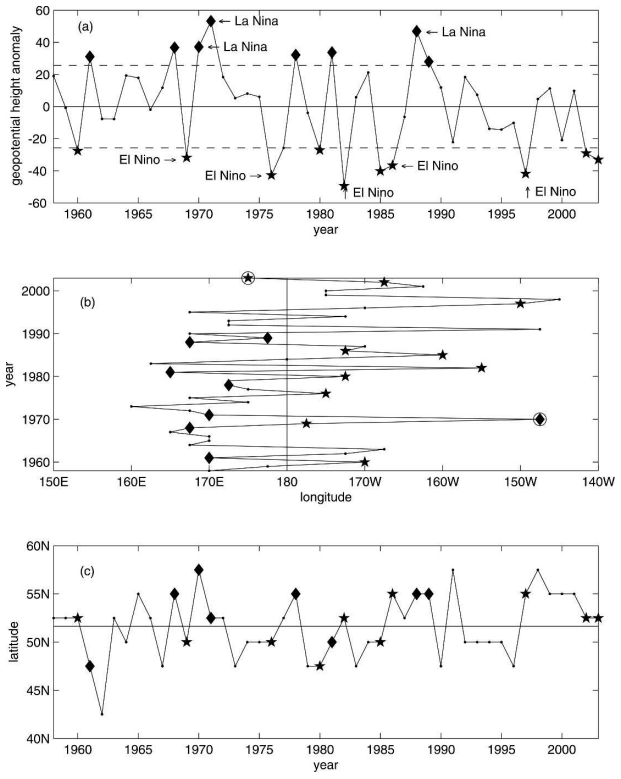

FIG. 2. Characteristics of the Aleutian low for 1958–2004. (a) Regional averaged 1000-hPa geopotential height anomaly in winter; based on 1958–2003 climatology. The dashed lines represent the standard deviation; (b) the longitude; and (c) latitude of the winter Aleutian low geopotential height minimum center. The pentagrams represent the position of the Aleutian low in strong years and the diamonds for weak years. The two circles in (b) represent the two exceptions noted in the text.

chosen to represent the years with a deeper Aleutian low (*strong years*), while the 1961/62, 1968/69, 1970/71, 1971/72, 1978/79, 1981/82, 1988/89, and 1989/90 winters were chosen to represent a shallower Aleutian low (*weak years*; Fig. 2a). Although Anderson and Gyakum (1989) suggested that much of the observed midlatitude interannual variance is generated internally without recourse to tropical forcing, it is still interesting to note that according to the definition of El Niño/La Niña years (Trenberth 1997; Coelho et al. 2005), half of the strong Aleutian low years (1969/70, 1976/1977, 1982/83, 1986/87, and 1997/98) were El Niño years and three of the weak Aleutian low years (1970/71, 1971/72, and 1988/89) were La Niña years (Fig. 2a).

When ascribing a location to the Aleutian low in a given winter, we identify the position of the minimum 1000-hPa geopotential height. In most of the sample years, the Aleutian low had only one minimum center. In our analysis, we encountered 12 winters (1958/59, 1964/65, 1966/67, 1967/68, 1968/69, 1970/71, 1971/72, 1973/74, 1974/75, 1975/76, 1981/82, and 1998/99) in which a split Aleutian low (i.e., one with two geopotential minimum centers) existed. In such split years, we identified the deepest center as the location of the Aleutian low. With only one exception, the longitude of the geopotential height minimum in strong years was east of the date line. Conversely, the weak years were characterized by a geopotential height minimum to the west of the date line with one exception (Fig. 2b). From the composite 1000-hPa geopotential height field for both strong and weak years (Figs. 3a,b), it is evident that the strong years were characterized by a deeper and eastward-shifted Aleutian low, while in the weak years the Aleutian low was shallower and westward shifted [Student's t test, degrees of freedom (df) = 259, $p < 0.01$] and split into two centers. The relationship between intensity and longitude of the Aleutian low is also noted in other studies (Trenberth 1990; Trenberth and Hurrell 1994; Overland et al. 1999). Note, however, that the latitude of the 1000-hPa geopotential height minimum in strong and weak years is not very different (Fig. 3). In fact, 6 of the 10 strong years occur north of the mean position, while 6 of the 8 weak years also occur north of the mean position (Fig. 2c).

In previous studies, cyclone detection has relied upon the identification of gridpoint SLP values surrounded by gridpoint values higher than the central point being tested (Serreze 1995; Serreze et al. 1997; McCabe et al. 2001; Zhang et al. 2004). The cyclone track is defined as the trajectory of the cyclone center and the cyclone intensity is defined as the mean absolute values of the difference between the central SLP of cyclones and the climatological monthly mean SLP at corresponding grid points over the cyclone duration (Zhang et al. 2004). For this study, a cyclone was defined as a minimum in the 1000-hPa geopotential height field surrounded by at least one closed isohypse (analyzed at 50-gpm intervals) for a minimum of 48 h. To emphasize the cyclone activity in the Aleutian low region, only those cyclones that moved into the selected region (40°–60°N, 150°E–140°W) at some point during their life cycles were considered. Using Lagrangian methods, the center or the minimum position of the cyclone in the daily 1000-hPa geopotential height field were tracked to show the characteristics of the cyclone track.

To measure the strength of each cyclone, we defined two cyclone intensity indices. *The gradient index* is defined, at the cyclone's mature stage, as the difference between the minimum 1000-hPa geopotential height in the cyclone center and the averaged 1000-hPa geopotential height of the surrounding eight points. *The circulation index* is defined as the sum of the 1000-hPa

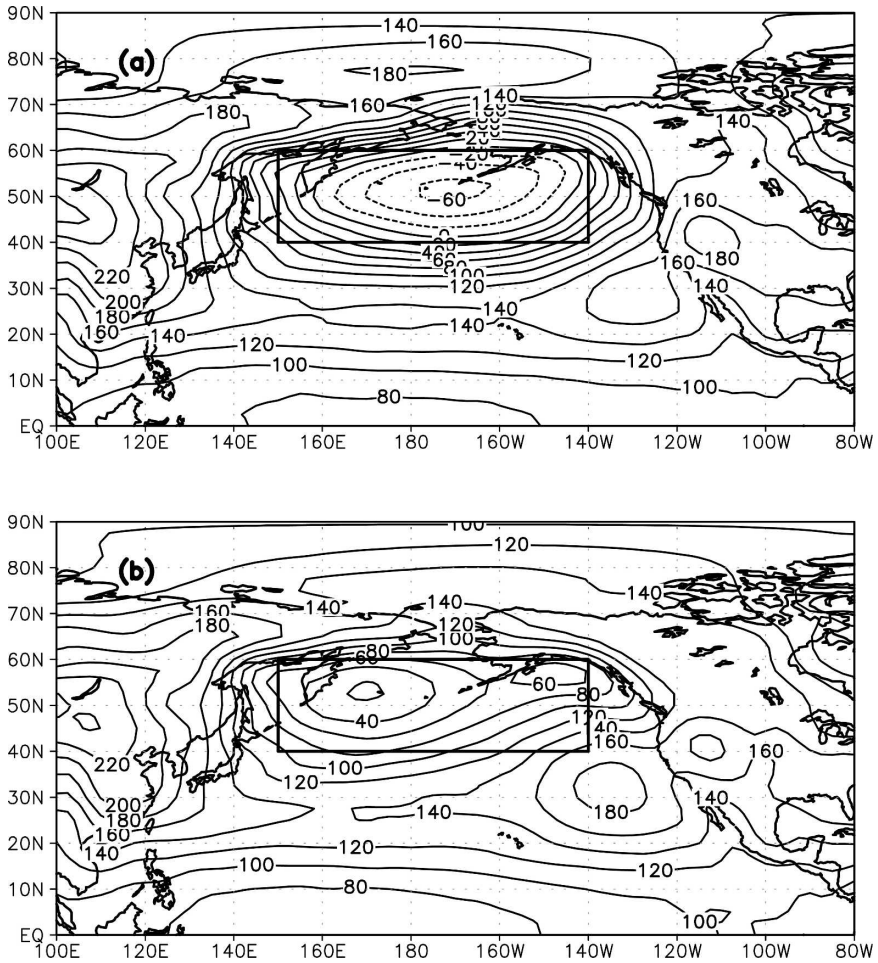

FIG. 3. Composite 1000-hPa geopotential height for (a) strong and (b) weak years (CI=20 gpm).

vorticity at the eight grid points surrounding the point of maximum 1000-hPa vorticity in the mature cyclone.

Some measure of cyclone size provides another discriminating characteristic of the cyclone activity. One fairly standard method of assessing cyclone size is to consider the area inside the last closed isohypse. In nature, however, the cyclone shape is often too complex to employ this method with ease. Striking a compromise between computational simplicity and physical accuracy, we suppose size can be assessed by considering successive squares around the central 1000-hPa geopotential minimum. The *square number* is then defined as the number of concentric squares that can be drawn around the geopotential minimum such that all grid values on each square exceed the grid values at all points on the preceding square. Employing this simple method, the square number can be transformed into an *area index* (squared kilometers) by the following formula:

$$\text{Area Index} = \sum_{n=1}^{n=\text{square number}\times 2-1} (2.5 \times 111) \times 2\pi R \times \cos[\phi - (\text{Square Number} \times 2.5) + (n-1) \times 2.5] \times \text{square number} \times 2 \times 2.5.$$

Here, 111 km is the approximate distance per degree of latitude, R is 6370 km, and ϕ is the latitude of the cyclone center.

3. Cyclone activity analysis

a. Cyclone frequency and cyclone duration

With the daily NCEP–NCAR reanalysis data, we tracked the winter cyclones in both strong and weak years, and found that the number of cyclones in each set of years was nearly equal (Table 1). The average num-

TABLE 1. The number and average number of the cyclone events in both strong and weak years.

	Strong yr										Weak yr							
Yr	1960	1969	1976	1980	1982	1985	1986	1997	2002	2003	1961	1968	1970	1971	1978	1981	1988	1989
No.	23	23	20	27	22	27	24	24	22	25	26	23	22	26	31	28	22	24
Avg				23.7										25.3				

ber of cyclone events in strong years was a bit smaller than in weak years.

The duration of the cyclone is defined as the time between the first and last closed isohypse, analyzed at 50-gpm intervals. The average duration of the cyclone in strong years is 6.8 days, and in the weak years was 6.4 days. The differences of cyclone duration between strong and weak years only pass the 74% significance level (Student's t test, df = 437, $p < 0.26$). But there were more cyclone cases with a duration longer than 12 days in strong years than in weak years (Fig. 4). About 23% of cyclone cases in weak years had a duration of 4 days, while only 12% of cyclone cases had 4 days' duration in strong years. This shows that although the mean cyclone duration is the same in both sets of years, there are more cyclones of long duration in strong years than in weak years.

b. Cyclone tracks

Although the frequency and the life span of the cyclone events in strong and weak years were somewhat similar, the tracks of the cyclones differed more drastically (Fig. 5). During the strong years, the cyclones moved along southwest–northeast tracks, which exhibit a more zonal tendency than their counterparts in weak years. The strong year tracks also appear to occur very close to one another. This kind of cyclone track distribution is similar to that described by Anderson and Gyakum (1989), which shows a well-defined zonal cyclone track maximum across the central Pacific with most occluded cyclones ending up near the Alaskan Peninsula and very few cyclones successfully reaching the west coast of North America. During the weak years, however, the cyclone tracks had a more poleward tendency and were spread throughout the whole North Pacific. Some spent more time in the northwest Pacific basin, finally reaching the Bering Sea, while others traveled to the Gulf of Alaska where they were occluded. Additionally, a few cyclones reached the west coast of North America.

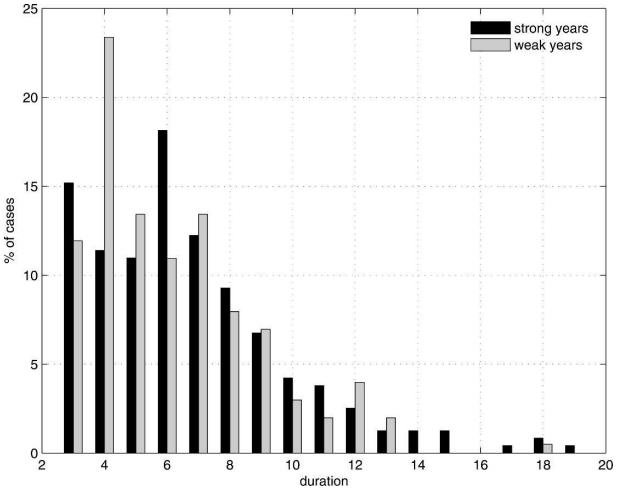

FIG. 4. Histograms of cyclone duration.

The cyclone tracks encompass the cyclogenesis, occlusion, and cyclolysis stages of the life cycle yet there were differences in the distributions of cyclones at these various stages. The cyclogenesis position was defined as the location at which the first closed 1000-hPa isohypse was identified, the mature[1] position shows the position of cyclone at its maximum intensity (as measured by the minimum 1000-hPa geopotential height), and the cyclolysis position refers to the location at which the last closed 1000-hPa isohypse was identified (Fig. 6). To better illustrate the characteristics of the cyclone track, the geographic distribution of the cyclone at the cyclogenesis, mature and cyclolysis stages is presented. Because there are 10 strong years and 8 weak years, the last 2 strong years (2002 and 2003) were ignored (Fig. 6).

The cumulative distribution of the cyclogenesis position for the entire 16 yr is shown in Fig. 6a. Cyclogenesis maximum regions in both years were in the eastern and the northern regions of Japan. Although these regions are favorable for cyclogenesis, some cyclogenesis occurred in the center of the North Pacific during the strong years. During the weak years, the cyclogenesis occurred in the region 30°–60°N, 130°–160°E, with a few appearing in the center of the North Pacific basin. The mean position of the cyclogenesis in strong years lies eastward of that in the weak years, and the varia-

[1] "Mature" is used to describe the stage in the life cycle at which the lowest geopotential height was observed.

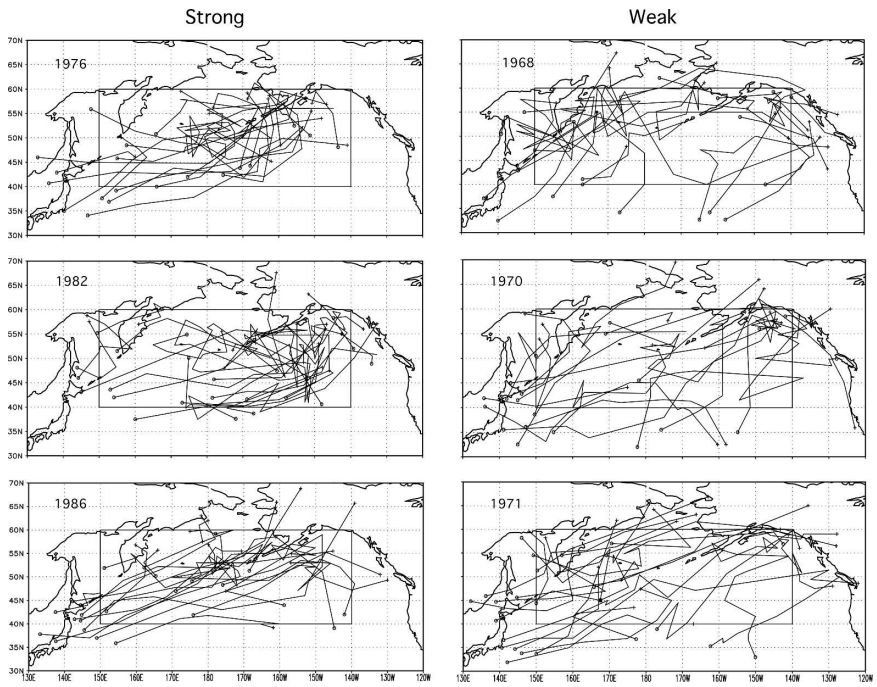

FIG. 5. North Pacific cyclone tracks in 6 yr. The samples of the (left) strong and (right) weak years. The unfilled circles represent the cyclogenesis positions, the filled circles represent the mature positions, the crosses represent the cyclolysis positions, and the unfilled squares represent the combining position of two or more cyclones.

tion of distribution in the north–south direction in the strong years is smaller than that in the weak years. The differences in longitude of cyclogenesis positions is at the 99% significance level using the Student's *t* test, while the differences in the latitude of the cyclogenesis positions has no significance. To show the details, we divided the whole region (130°E–120°W) into 10° longitude intervals and counted the cyclone number in each of the 11 small regions. Cyclogenesis in both types of years has a peak in 140°–160°E longitude channel. However, there are more cyclogenesis events in strong years than in weak years in the 170°E–170°W region (Fig. 6a), which means that cyclogenesis in the center of the Pacific was more common in the strong years than in weak years.

The traveling cyclones usually reach maximum intensity in the area of the Aleutian low. At the mature stage, most of the cyclones appeared in the center of the Aleutian low region (Fig. 6b). The mean position of mature cyclones in strong years was southeast of that in weak years and the standard deviation of the position in strong years was smaller than that in the weak years. [The differences in longitude (latitude) of the mature positions are at the 99% (95%) significance level using the Student's *t* test.] During the strong years, most mature cyclones were concentrated to the east of the date line, especially near the Alaska Peninsula. Conversely, most mature cyclones were scattered to the west of the date line during the weak years. The longitudinal binning also shows that the favorite region for mature cyclones in the strong years was from 180° to 160°W, while the favorite region in weak years was from 160°E to 180° (Fig. 6b).

Figure 6c shows that the cyclolysis position in both groups were similar to those found by Martin et al. (2001), who concluded that the Gulf of Alaska and Northwest Pacific are the primary regions for the cyclolysis and that the Bering Sea is the secondary region. The differences in the longitude (latitude) of cyclolysis positions are at only the 36% (40%) significance level by the Student's *t* test. However, strong years' cyclolysis and weak years' cyclolysis distribution exhibited some differences. During the strong years, some of the cyclones decayed in the Bering Sea, some of them decayed in the Northwest Pacific, but most decayed in the Gulf of Alaska. Only a few decayed along the west coast of North America. The cyclolysis position in strong years is concentrated in 170°–140°W longitude channel. The decay of the weak year cyclones, showing a relative peak in 140°–130°W longitude channel (Fig. 6c), was not concentrated in a region, but instead occurred in many different positions (Fig. 6c).

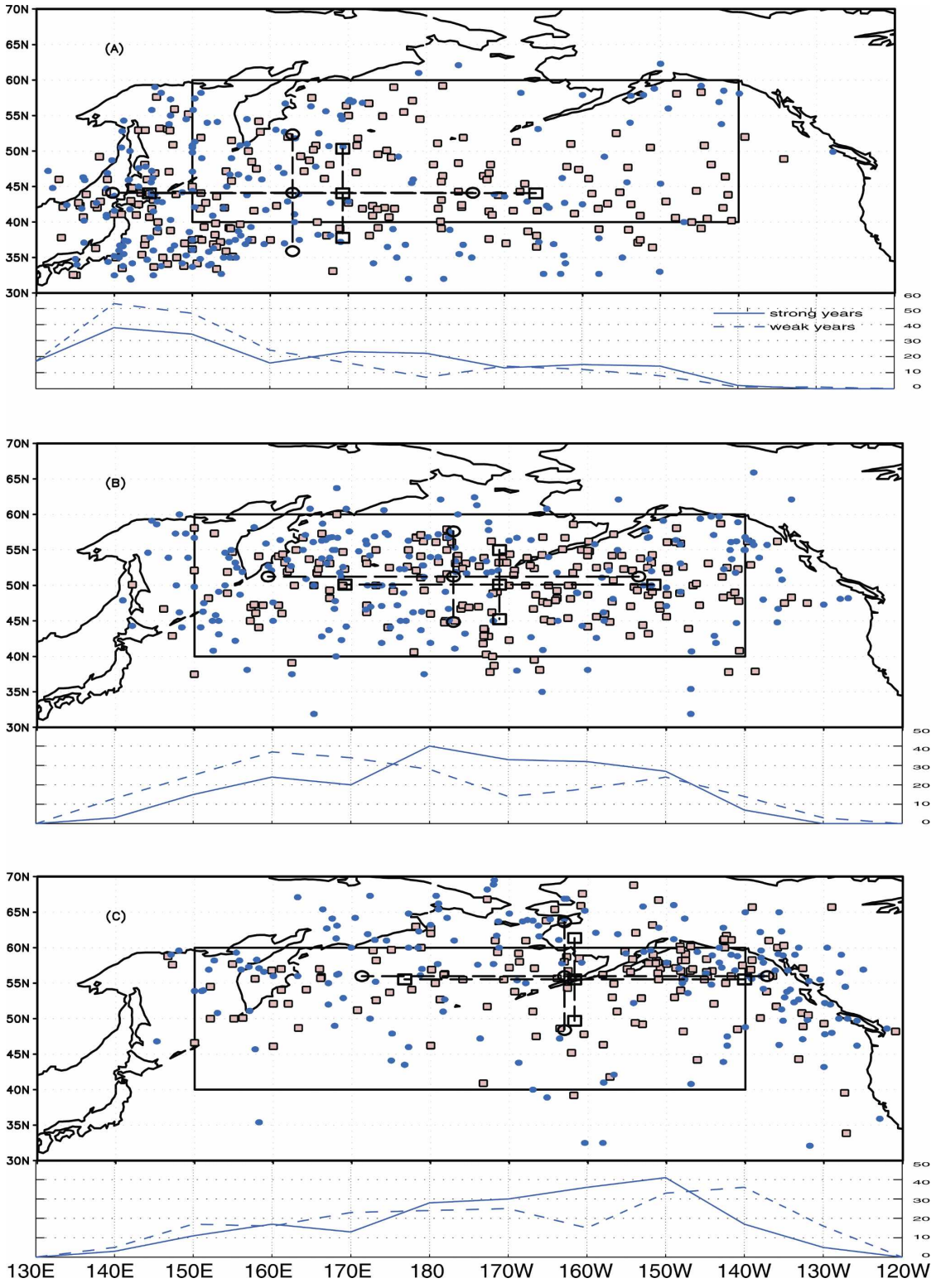

FIG. 6. Distributions and histograms of the (a) cyclogenesis, (b) mature, and (c) cyclolysis positions for strong and weak years. The filled squares represent the strong years and the unfilled squares represent the mean position and the mean position minus or plus the standard deviation in strong years, while the filled circles represent the weak years and the unfilled circles are the same as the unfilled squares but for the weak years. In the histogram, the solid line represents cyclone number in each small region in strong years, while the dashed line represents the same quantity in weak years.

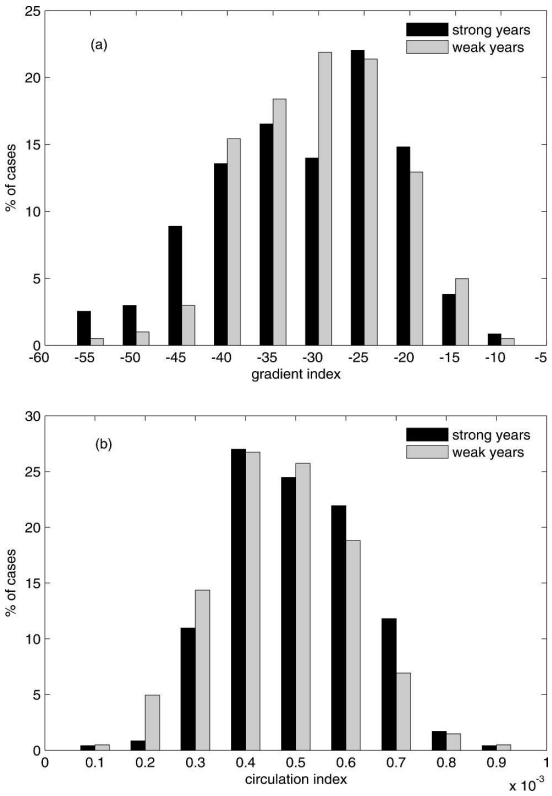

FIG. 7. Histograms of the (a) gradient and (b) circulation indexes.

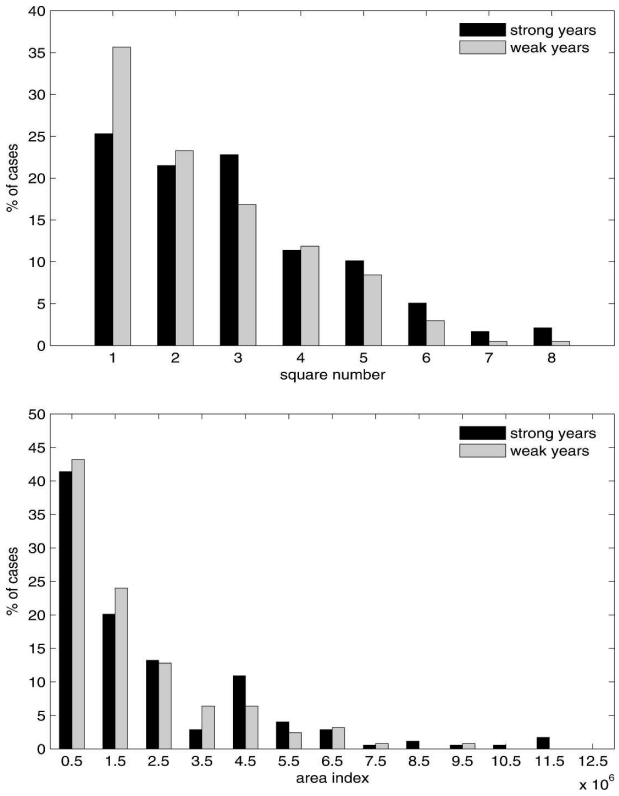

FIG. 8. Histograms of the (a) square number and the (b) area index.

c. *Cyclone intensity*

Cyclones generally deepen from the cyclogenesis stage to the mature stage, and weaken from the mature stage to the cyclolysis stage. Consequently, the cyclone intensity is estimated using the gradient index and the circulation index at the mature stage. The mean gradient index in strong years was −28.8 gpm, while in the weak years it was −27.8 gpm (Student's t test, df = 437, $p < 0.32$). But individually speaking, there were more cyclone cases with the gradient index below −40 gpm in strong years than in weak years (Fig. 7a). Conversely there were fewer cyclone cases with the gradient index between −40 and −25 gpm in strong years than in weak years. From this, we conclude that there are more intense cyclone cases in strong years than in weak years. A similar conclusion can be drawn from the analysis of the circulation index that represents a measurement of the average vorticity around the maximum vorticity grid point, or the strength of the cyclone. The mean circulation index in strong years was 5.48×10^{-4} s^{-1}, while it was 5.20×10^{-4} s^{-1} in weak years. These differences were only at the 95% significance level (Student's t test, df = 437). A comparison of the histograms of circulation index shows that there were more cyclone cases with a large circulation index in strong years than in weak years, especially of the cases with circulation index above 5.0×10^{-4} s^{-1} (Fig. 7b).

d. *Cyclone size*

The strong year cyclones were characterized by a mean square number of 2.94 loops and mean area index of 2 073 700 km^2, while the weak year cyclones only had a mean square number of 2.50 loops and mean area index of 1 446 600 km^2. These differences were at the 99% significance level (Student's t test, df = 437). This shows that the mature cyclone in strong years covered a larger area than its counterpart in weak years. There were more cyclones with larger square number in strong years than in weak years, especially of cases with the square number above five loops (Fig. 8a) and the area index larger than 4 500 000 km^2 (Fig. 8b). The whole Aleutian low region (40°–60°N, 150°E–140°W) is about 11 335 000 km^2. However, 2% of cyclone cases in stronger years were characterized by the cyclone size larger than 11 500 000 km^2, while no cyclones larger than that occurred in weak years (Fig. 8b). Clearly,

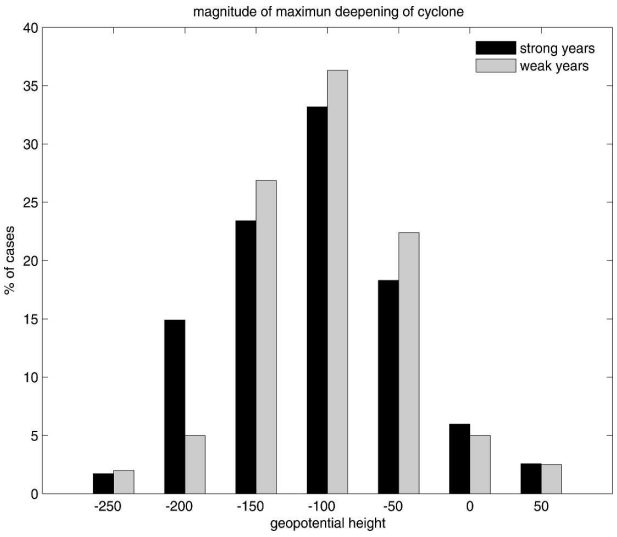

FIG. 9. Histograms of magnitude of maximum cyclone deepening.

there are more large cyclone cases in strong years than in weak years.

e. Maximum cyclone deepening

To better illustrate cyclone development, we analyze the maximum cyclone deepening rate. The cyclone deepening is defined as the 1000-hPa geopotential height difference at the center of a given cyclones between successive charts. The mean magnitude of maximum cyclone deepening was -108.5 gpm day^{-1} in strong years and -97.06 gpm day^{-1} in weak years. Maximum cyclone deepening smaller than -200 gpm day^{-1} was much more common in strong years than in weak years (Fig. 9). Using the Student's t test, the difference in deepening rates between strong and weak years was significant at the 95% level (df = 437) demonstrating that cyclone intensification in strong years is much more pronounced than in weak years. The location of the maximum cyclone deepening (not shown) indicates that the mean position in strong years was located east of the mean position in weak years. In about 62% (63%) of cyclone cases in strong (weak) years the maximum cyclone deepening position was nearly the same as the cyclogenesis position. The remaining 38% (37%) were located near the mature position.

4. Composite large-scale circulation condition

a. Midtropospheric conditions

In the midtroposphere, the strong years were characterized by a negative geopotential height anomaly along with a cyclonic circulation anomaly over the North Pacific (Fig. 10a). However, the weak years were characterized by a positive geopotential height anomaly associated with an anticyclonic circulation anomaly in the Aleutian low region (Fig. 10b). The shift of the height field was accompanied by a change in the wind field pattern. The wind in strong years was characterized by the stronger and more zonal wind with small meridional component west of 160°W. A large meridional component was shown only in the Gulf of Alaska and near the west coast of the North America (Fig. 10c). The wind in weak years was somewhat weaker and had a more meridional component west of 160°W. Moreover the region with maximum meridional wind component appeared west of 160°W (Fig. 10d). During the strong years, the zonal wind flowed from East Asia to 160°W before backing to the southwest and flowing toward the Gulf of Alaska. The flow in the center of the Aleutian low region was very weak. Under the influence of the 500-hPa wind, which effectively acts as the steering wind, the cyclones preferred to travel with more zonal tracks, most in the northeast Pacific traveled toward Alaska. The steering wind in weak years, however, flowed from East Asia to the Bering Sea and the Gulf of Alaska with the maximum meridional component in the center of the Aleutian low region. With this steering wind, some of the cyclones traveled from East Asia to the Bering Sea, some to the Gulf of Alaska, and others to the west coast of North America.

b. Upper-tropospheric conditions

In the upper troposphere, the strong years were characterized by a narrow high-amplitude ridge over the west coast of the North America and by a broad trough across the northwest Pacific (Fig. 11a). Associated with the broad trough in strong years, an intense, zonally elongated jet extended across most of the Pacific basin (Fig. 11c). In strong years, the region of wind speeds larger than 30 m s^{-1} was elongated to 140°W. Weak years were associated with a westward shifted, broad ridge across the eastern Pacific and a narrow trough over eastern Asia (Fig. 11b). But in weak years, a weaker, zonally retracted jet over East Asia was consistent with the narrow trough (Fig. 11d). The climatological Aleutian low center was east of the date line in strong years, while the Aleutian low center was east of the date line in the weak years (Fig. 3a). With the retracted jet only reaching 170°W, the Aleutian low center was to the west of the date line in weak years (Fig. 3b). Associated with the elongated jet in strong years, the strong year mean cyclogenesis and mature positions are to the east of their counterparts in weak years (Fig. 11).

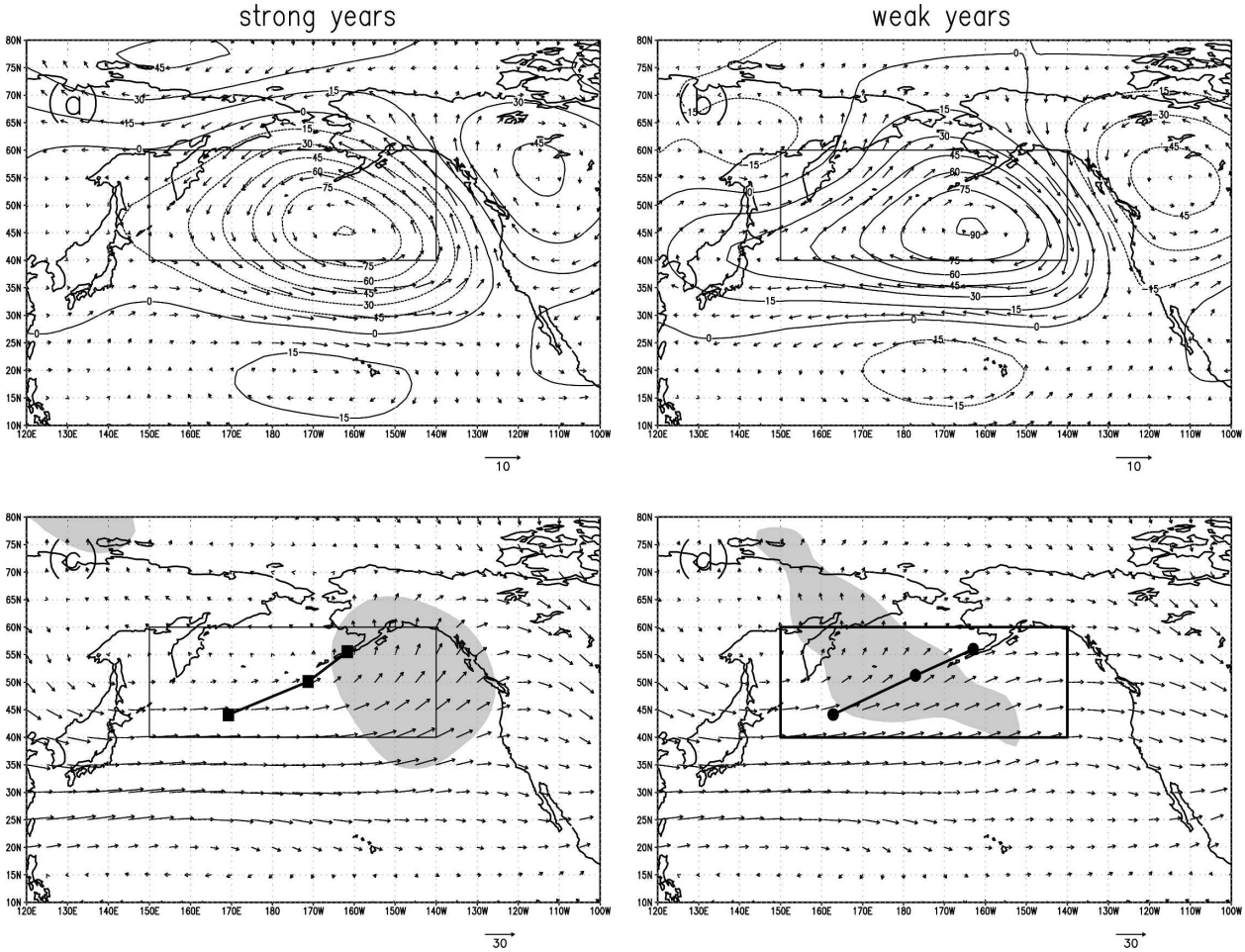

FIG. 10. Composite 500-hPa geopotential height anomaly (CI = 40 gpm) and wind anomaly for (a) strong and (b) weak years and composite 500-hPa wind field for (c) strong and (d) weak years. The standard wind vector represents 30 m s^{-1} and shaded is for meridional wind speed above 5 m s^{-1}. The filled squares in (c) represent the mean cyclogenesis, mature, and cyclolysis position in strong years and the filled circles in (d) represent the weak years.

c. Waveguide

The stationary barotropic Rossby wavenumber, K_s, is a useful diagnostic index for representing the mean large-scale circulation state (Hoskins and Ambrizzi 1993; Yang and Hoskins 1996; Kiladis 1998; Matthew and Kiladis 1999; Otkin and Martin 2004b). The waveguide nature of subtropical jets can be seen from the axes of maximum stationary wavenumber that lie along the jet axes, especially in the Asian–Pacific jet (Matthew and Kiladis 1999). The wavenumber K_s at which a barotropic Rossby wave is stationary at a particular location in a given background zonal flow is defined as $K_s = \sqrt{(\beta_*/\overline{U})}$, where $\beta_* = \beta - (\partial^2\overline{U}/\partial y^2)$ is the meridional gradient of absolute vorticity and $\overline{U}$ is the time-mean zonal wind. A real value for K_s is possible if the flow is westerly (positive $\overline{U}$) and β_* is positive. Hoskins and Ambrizzi (1993) proved that Rossby rays are always refracted toward latitudes with larger K_s, indicating that a K_s maximum provides a Rossby waveguide. During strong years, a continuous band of stationary wavenumber, K_s, is associated with the zonally elongated Asian jet and the band splits only near the west coast of the North America (Fig. 12a). This suggests that during strong years the jet acts as an effective waveguide that strongly mandates the zonal propagation of cyclones. However, during the weak years, the waveguide appeared to be less well organized; it split in the central Pacific and induced the meridional propagation of the cyclones in the northeast Pacific (Fig. 12b).

d. Eady growth rate index

Blackmon et al. (1977) gave a schematic illustration of the cross sections transverse to the jet stream. In the exit region of the jet, there is a strong equatorward

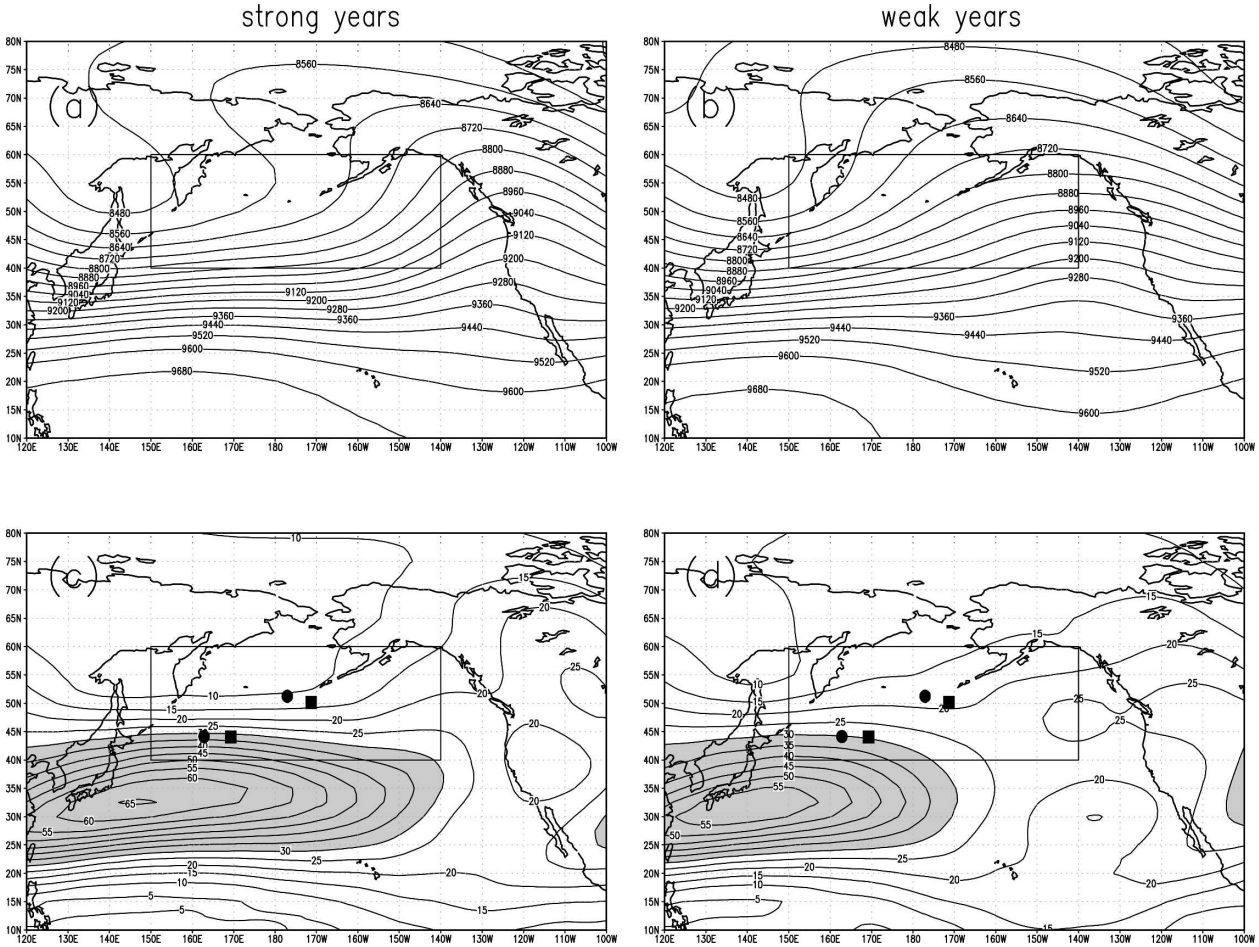

FIG. 11. Composite 300-hPa geopotential height for (a) strong and (b) weak years (CI = 80 gpm) and composite 300-hPa wind speed field for (c) strong and (d) weak years (CI = 5 m s^{-1}), shaded for values above 30 m s^{-1}. The filled squares are the mean cyclogenesis and mature position in strong years, while the filled circles are for weak years.

ageostrophic flow in the upper troposphere while in the lower troposphere, there is a strong poleward heat flux that provides a favorable condition for cyclogenesis. During the strong years, the exit region of the jet core extended across most of the Pacific basin, which provided a favorable condition for cyclogenesis and the development of the cyclone in the center of the Aleutian low region. However, the zonal extent of the jet in weak years only reached to 170°W. Consequently, few cyclones developed in the eastern North Pacific. The Eady growth rate index is used to provide a measure of the baroclinic instability, a necessary condition for cyclone growth (Hoskins and Valdes 1990; Hall et al. 1994; Paciorek et al. 2002). The daily Eady growth rate index, σ_{BI} is defined as $\sigma_{BI} = 0.31(f/N)|(\partial \mathbf{V}/\partial z)|$, where f is the Coriolis parameter, N is the buoyancy frequency, and $\mathbf{V}$ is the horizontal wind (Hoskins and Valdes 1990; Hall et al. 1994; Paciorek et al. 2002). The buoyancy frequency is calculated from $N^2 = (g/\theta)(\partial\theta/\partial z)$, where g is the gravity and θ is the potential temperature. Hoskins and Valdes (1990) calculated the Eady growth rate index at 780 hPa, while Paciorek et al. (2002) calculate the Eady growth rate index at 500 hPa. In the present study, we consider the vertical wind shear in the 400–600-hPa layer and, consequently, we refer to the Eady growth rate index at 500 hPa.

Figure 13 shows the distribution of Eady growth rate index in the North Pacific. The maximum Eady growth rate index in both strong and weak years is located in the Kuroshio and its extension region. The low static stability (associated with the presence of the Kuroshio) and the large vertical shear (associated with the Asian jet) provide fertile ground for cyclone growth in this region in support of the observations that most of the cyclones are generated here (Fig. 6a) and most of the cyclones passing through the area of the Kuroshio intensified in this region (Gyakum et al. 1989). The strength and position of the center in strong years is

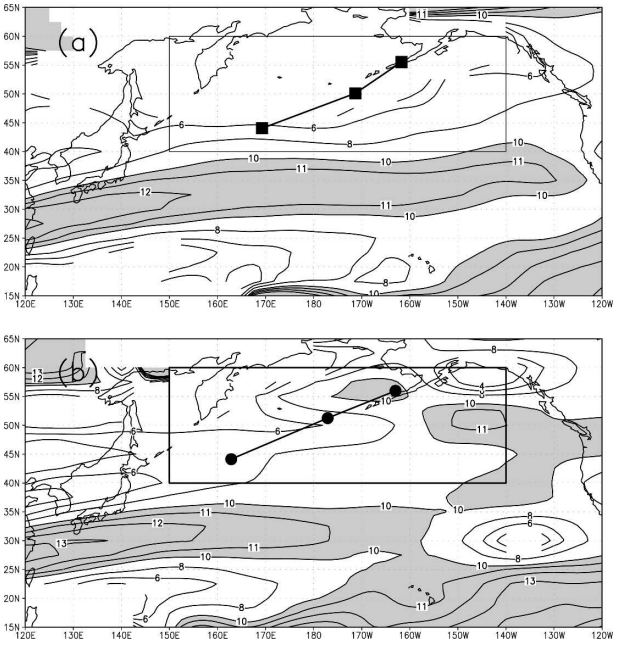

FIG. 12. Stationary wavenumber K_s calculated from the 300-hPa zonal wind for (a) composite strong years and (b) composite weak years (CI = 2). Shading is for values above 10. The default regions indicate the easterly wind region or the regions where β_* is negative. The filled squares represent the mean cyclogenesis, mature, and cyclolysis position in strong years, while the filled circles represent the weak years.

larger and extends farther eastward than in the weak years. The belt with values above 0.85 day^{-1} was elongated to 160°W in strong years (Fig. 13a), while it was retracted to west of date line in weak years (Fig. 13b). The more eastward extended Eady growth rate center in strong years is consistent with the fact that the mean cyclogenesis position was more eastward than in weak years (Fig. 13). The elongated high baroclinity belt in strong years also provided a favorable condition for cyclone growth in the central Pacific. These large-scale conditions account for the more frequent cyclogenesis in ~170°E–170°W longitude channel in the strong years. Consequently, more mature cyclones appeared to the east of date line.

5. Discussion

On a daily weather map, there are alternating cyclones and anticyclones moving generally to the east in the area of the Aleutian low. It is not the scene of an intense stationary low. The Aleutian low is truly only a low pressure system *on average*. This being the case, then there are two rather simple conceptualizations that might account for deepening the Aleutian low. One is directly a result of the cyclone activity. Suppose the background geopotential height field experiences little or no temporal change. In such a case, the Aleutian low deepens only when transient, deepening cyclones occupy the region of the Aleutian low. Alternatively, it is possible that the background geopotential height field gradually deepens as the winter progresses. If such gradual, large-scale deepening is superposed with a parade of cyclone events of nearly uniform intensity, the Aleutian low will also deepen significantly.

Given these distinct possibilities, an estimate of the impact of cyclone variability on the interannual variability of Aleutian low intensity can be made. The variability in cyclone intensity can be estimated as $R = [(\Delta p_s - \Delta p_w)/(\Delta p_s + \Delta p_w)/2)]100\%$, where $\Delta p_s(\Delta p_w)$ is the average gradient index for all cyclones in strong (weak) years, calculated as

$$\Delta p_s = \frac{\sum_{n=1}^{10}\left[\sum_{\text{each mature cyclone in one year}} (\text{gradient index} \times \text{duration} \times \text{area index})\right]}{10}$$

$$\Delta p_w = \frac{\sum_{n=1}^{8}\left[\sum_{\text{each mature cyclone in one year}} (\text{gradient index} \times \text{duration} \times \text{area index})\right]}{8}.$$

The variability in the intensity of the Aleutian low can be estimated as $R_c = (\Delta p_{cs} - \Delta p_{cw}/\Delta p_c) \times 100\%$, where $\Delta p_{cs}(\Delta p_{cw})$ is the geopotential height difference between the average geopotential height along the perimeter of the region 30°–70°N, 130°E–120°W and the minimum geopotential height of the Aleutian low in the composite 1000-hPa geopotential height field for strong (weak) years. Here Δp_c represents a similar quantity for the climatological wintertime Aleutian low. Measured in this way, the relative change of cyclone intensity, R, was about 33%, while the relative change of Aleutian low intensity, R_c, was about 46%. Consequently, the ratio of the two relative changes was 73%, suggesting that the interannual variability of cyclone intensity may

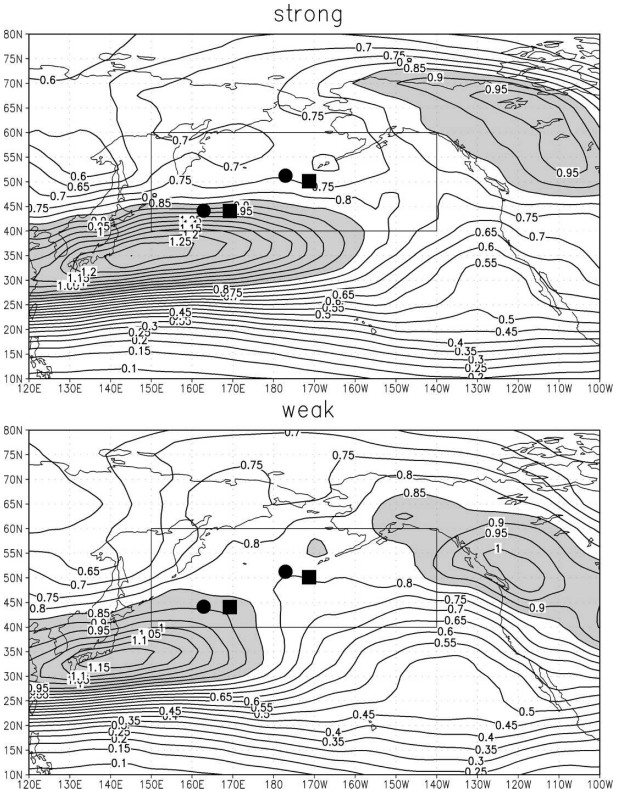

FIG. 13. Composite mean fields for Eady growth rate index in (a) strong and (b) weak years (CI = 0.05 day^{-1}); shading is for values above 0.85 day^{-1}. The filled squares represent the mean cyclogenesis and mature position in the strong years and the filled circles represent the weak years.

be a significant driver of changes in the intensity of the Aleutian low.

6. Summary and conclusions

In this work, winter cyclone activity within the Aleutian low region 40°–60°N, 150°E–140°W is studied. Employing the standard deviation of the regional averaged 1000-hPa geopotential height, strong and weak Aleutian low years were identified. The strong years consist of 10 winters (1960/61, 1969/70, 1976/77, 1980/81, 1982/83, 1985/86, 1986/87, 1997/98, 2002/03, and 2003/04), while there are 8 weak winters (1961/62, 1968/69, 1970/71, 1971/72, 1978/79, 1981/82, 1988/89, and 1989/90). A system-centered Lagrangian method is used to track individual cyclone centers throughout these winters.

From the statistical analysis of the cyclone activity, we find that cyclone events occurred in almost the same number in the two groups of years and that the average cyclone duration is nearly the same with a slightly longer cyclone life span in strong years, while there are more cyclone events of particularly long duration in strong years than in weak years. Also, the mean state of cyclone intensity in both sets of years was almost the same as measured by the gradient index and the circulation index. But there were more cases of especially strong cyclones in strong years than in weak years.

However, three other features of the cyclone activity exhibit great differences between strong years and weak years. One robust difference is in the track direction and tendency. During the strong years, the cyclones moved with more zonal tracks and most of the cyclone tracks were very close to each other. Associated with the clustered southwest–northeast cyclone track, the cyclogenesis and mature cyclone positions were located farther east and were more spatially concentrated in strong years than in weak years. Additionally, the favorable region for cyclolysis in strong years is the Gulf of Alaska with only a few cyclolysis events identified on the west coast of the North America. During the weak years, the cyclone tracks displayed a more poleward tendency and were more widely distributed throughout the whole North Pacific basin, accompanied by a much wider range of cyclogenesis, mature, and cyclolysis positions than in strong years. The second significant difference is in the cyclone size. It was found that the mean area index in strong years is 627 100 km^2 larger than in weak years, with 2% of cyclone cases in strong years actually larger than the Aleutian low. This shows that the mature cyclones in strong years cover a larger area than those in weak years and more large cyclones occur in strong years than in weak years. Another significant difference is in the deepening of individual cyclones. The mean magnitude of maximum cyclone deepening in strong years was larger than that in weak years. Also, maximum cyclone deepening in excess of -200 gpm day^{-1} occurred more frequently in strong years than in weak years, demonstrating that cyclone intensification in strong years is much stronger than that in weak years.

Accordingly, the large-scale circulation exhibits some differences between both sets of years. The strong years were characterized by a broad trough across the North Pacific accompanied by strong zonal wind with small meridional component west of 160°W. The weak years, however, were characterized by a narrow trough over East Asia accompanied by winds with a significant meridional component west of 160°W. In the middle troposphere, the geostrophic wind fields may play a role as the steering wind. As a result, cyclone activity in strong years exhibited more zonal tracks than those in weak years. In addition, with the southwesterly steering wind in the eastern North Pacific, the cyclones traveled almost as far as the Gulf of Alaska in strong years, while in weak years a southwesterly steering wind appears in

the center of the North Pacific. As a consequence, weak year cyclones had a tendency to migrate toward the Bering Sea. Associated with the stronger and more zonally elongated jet in strong years, the band of maximum waveguide extending across the Pacific is more zonally elongated in strong years than in weak years, which limits the meridional propagation of the cyclones in strong years. Additionally, the elongated high baroclinity belt of Eady growth rate index above 0.85 day^{-1} stretched eastward to 160°W in strong years, providing a favorable condition for cyclone growth in the central Pacific. Therefore, the large-scale circulation provided more favorable conditions for more zonal cyclone tracks and for more mature cyclones appearing to the east of date line in strong years than in weak years.

Since it is a statistical entity, two possible mechanisms may underlie the variations in the intensity of the Aleutian low. The Aleutian low may be intensified as a result of 1) the steady progression of ever more intense cyclones through the Aleutian low region as the winter progresses, or 2) a gradually deepening background state during winter superimposed with a parade of cyclones of steady intensity through the season. The relative change of cyclone intensity accounts for about 73% of the relative change of Aleutian low intensity in the winter months. Though more sophisticated examination is clearly needed, we suggest that the variability of cyclone intensity may be a significant driver of Aleutian low evolution.

It has long been recognized that the climate system exerts an influence on cyclone activity. The results presented here suggest that synoptic cyclone activity, in turn, plays an important role in shaping the large-scale atmospheric circulation and its feedback on the climate system. Many climate model analyses work with monthly data while ignoring the higher-frequency synoptic systems. These higher-frequency features may exert very important controls on a number of different atmospheric responses. It has become increasingly apparent that the study of synoptic scales requires some consideration of the climate system. Equally, no reasonable study of the behavior of the climate system, especially on interannual time scales, can be made without reference to the behavior of synoptic-scale weather systems.

Acknowledgments. The authors thank the NOAA–CIRES Climate Diagnostics Center for providing the NCEP–NCAR reanalysis data (available online at http://www.cdc.noaa.gov/). We also thank Dr. E. DeWeaver for helpful discussions and Erika Millstein for editorial assistance. We want to express our gratitude for support From the National Natural Science Foundation of China (Grant 40333030), the National Basic Research Program of China (Grant 2005CB422301), and the Education Ministry of China. This work was also supported partially by the U.S. Department of Energy and NOAA.

REFERENCES

Alexander, M. A., 1992: Midlatitude atmosphere–ocean interaction during El Niño. Part I: The North Pacific Ocean. *J. Climate,* **5,** 944–958.

Anderson, J. R., and J. R. Gyakum, 1989: A diagnostic study of Pacific basin circulation regimes as determined from extra−tropical cyclone tracks. *Mon. Wea. Rev.,* **117,** 2672–2686.

Blackmon, M. L., 1976: A climatological spectral study of the 500 mb geopotential height of the Northern Hemisphere. *J. Atmos. Sci.,* **33,** 1607–1623.

——, J. M. Wallace, N.-C. Lau, and S. L. Mullen, 1977: An observational study of the Northern Hemisphere wintertime circulation. *J. Atmos. Sci.,* **34,** 1040–1053.

Chen, T.-C., H. Van Loon, K.-D. Wu, and M.-C. Yen, 1992: Change in the atmospheric circulation over the North Pacific–North America area since 1950. *J. Meteor. Soc. Japan,* **70,** 1137–1146.

Coelho, C. A. S., D. B. Stephenson, J. D.-R. Francisco, and M. Balmaseda, 2005: From multi-model ensemble predictions to well-calibrated probability forecasts: Seasonal rainfall forecasts over South America 1959–2001. *CLIVAR Exchanges,* No. 10, International CLIVAR Project Office, Southampton, United Kingdom,14–20.

Gyakum, J. R., J. R. Anderson, R. H. Grumm, and E. L. Gruner, 1989: North Pacific cold-season surface cyclone activity: 1975–1983. *Mon. Wea. Rev.,* **117,** 1141–1155.

Hall, N., B. Hoskins, P. Valdes, and C. Senior, 1994: Storm tracks in a high-resolution GCM with doubled carbon dioxide. *Quart. J. Roy. Meteor. Soc.,* **120,** 1209–1230.

Hartmann, B., and G. Wendler, 2005: The significance of the 1976 Pacific climate shift in the climatology of Alaska. *J. Climate,* **18,** 4824–4839.

Hodges, K. I., 1995: Feature tracking on the unit sphere. *Mon. Wea. Rev.,* **123,** 3458–3465.

——, 1999: Adaptive constraints for feature tracking. *Mon. Wea. Rev.,* **127,** 1362–1373.

Hoskins, B. J., and P. J. Valdes, 1990: On the existence of storm tracks. *J. Atmos. Sci.,* **47,** 1854–1864.

——, and T. Ambrizzi, 1993: Rossby wave propagation on a realistic longitudinally varying flow. *J. Atmos. Sci.,* **50,** 1661–1671.

——, and K. I. Hodges, 2002: New perspectives on the Northern Hemisphere winter storm tracks. *J. Atmos. Sci.,* **59,** 1041–1061.

——, I. N. James, and G. H. White, 1983: The shape, propagation, and mean-flow interaction of large-scale weather systems. *J. Atmos. Sci.,* **40,** 1595–1612.

Kiladis, G. N., 1998: Observations of Rossby waves linked to convection over the eastern tropical Pacific. *J. Atmos. Sci.,* **55,** 321–339.

Klein, W. H., 1957: Principal tracks and mean frequencies of cyclones and anticyclones in the Northern Hemisphere. Research Paper 40, U.S. Weather Bureau, 60 pp.

Koning, W., R. Sausen, and E. Sielman, 1993: Objective identifi-

cation of cyclones in GCM simulation. *J. Climate,* **6,** 2217–2231.

Lambert, S. J., 1995: The effect of enhanced greenhouse warming on winter cyclone frequencies and strengths. *J. Climate,* **8,** 1447–1452.

Latif, M., and T. P. Barnett, 1996: Decadal climate variability over the North Pacific and North America: Dynamics and predictability. *J. Climate,* **9,** 2407–2423.

Lau, N.-C., 1988: Variability of the observed midlatitude storm tracks on relation to low-frequency change in the circulation pattern. *J. Atmos. Sci.,* **45,** 2718–2743.

——, and M. J. Nath, 1994: A modeling study of the relative roles of tropical and extratropical SST anomalies in the variability of the global atmosphere–ocean system. *J. Climate,* **7,** 1184–1207.

Mantua, N. J., S. R. Hare, Y. Zhang, J. M. Wallace, and R. C. Francis, 1997: A Pacific interdecadal climate oscillation with impacts on salmon production. *Bull. Amer. Meteor. Soc.,* **78,** 1069–1079.

Martin, J. E., R. D. Grauman, and N. Marsili, 2001: Surface cyclolysis in the North Pacific Ocean. Part I: A synoptic climatology. *Mon. Wea. Rev.,* **129,** 748–765.

Matthew, A. J., and G. N. Kiladis, 1999: The tropical–extratropical interaction between high-frequency transients and the Madden–Julian oscillation. *Mon. Wea. Rev.,* **127,** 661–677.

McCabe, G. J., P. C. Martyn, and M. C. Serreze, 2001: Trends in Northern Hemisphere surface cyclone frequency and intensity. *J. Climate,* **14,** 2763–2768.

Murray, R. J., and I. Simmonds, 1991a: A numerical scheme for tracking cyclone centers from digital data. Part I: Development and operation of the scheme. *Aust. Meteor. Mag.,* **39,** 155–166.

——, and ——, 1991b: A numerical scheme for tracking cyclone centers from digital data. Part II: Application to January and July GCM simulations. *Aust. Meteor. Mag.,* **39,** 167–180.

Otkin, J. A., and J. E. Martin, 2004a: A synoptic climatology of the subtropical Kona storm. *Mon. Wea. Rev.,* **132,** 1502–1517.

——, and ——, 2004b: The large-scale modulation of subtropical cyclogenesis in the central and eastern Pacific Ocean. *Mon. Wea. Rev.,* **132,** 1813–1828.

Overland, J. E., J. M. Adams, and N. A. Bond, 1999: Decadal variability of the Aleutian low and its relation to high-latitude circulation. *J. Climate,* **12,** 1542–1548.

Paciorek, C. J., J. S. Risbey, V. Ventura, and R. D. Rosen, 2002: Multiple indices of Northern Hemisphere cyclone activity, winters 1949–99. *J. Climate,* **15,** 1573–1590.

Palmer, T. N., 1998: Nonlinear dynamics and climate change: Rossby's legacy. *Bull. Amer. Meteor. Soc.,* **79,** 1411–1423.

Rodionov, S. N., J. E. Overland, and N. A. Bond, 2005: The Aleutian low and winter climate conditions in the Bering Sea. Part I: Classification. *J. Climate,* **18,** 160–177.

Sawyer, J. S., 1970: Observational characteristics of atmospheric fluctuations with a time scale of a month. *Quart. J. Roy. Meteor. Soc.,* **96,** 610–625.

Schneider, N., and B. D. Cornuelle, 2005: The forcing of the Pacific decadal oscillation. *J. Climate,* **18,** 4355–4373.

Serreze, M. C., 1995: Climatological aspects of cyclone development and decay in the Arctic. *Atmos.–Ocean,* **33,** 1–23.

——, F. Carse, R. G. Barry, and J. C. Rogers, 1997: Icelandic low cyclone activity: Climatological features, linkages with the NAO, and relationships with recent changes in the Northern Hemisphere circulation. *J. Climate,* **10,** 453–464.

Sinclair, M. R., J. A. Renwick, and J. W. Kidson, 1997: Low-frequency variability of Southern Hemisphere sea level pressure and weather system activity. *Mon. Wea. Rev.,* **125,** 2531–2543.

Trenberth, K. E., 1986: An assessment of the impact of transient eddies on the zonal flow during a blocking episode using localized Eliassen–Palm flux diagnostics. *J. Atmos. Sci.,* **43,** 2070–2087.

——, 1990: Recent observed interdecadal climate changes in the Northern Hemisphere. *Bull. Amer. Meteor. Soc.,* **71,** 988–993.

——, 1997: The definition of El Niño. *Bull. Amer. Meteor. Soc.,* **78,** 2771–2777.

——, and J. W. Hurrell, 1994: Decadal atmosphere–ocean variations in the Pacific. *Climate Dyn.,* **9,** 303–319.

——, and D. P. Stepaniak, 2003: Seamless poleward atmospheric energy transports and implications for the Hadley circulation. *J. Climate,* **16,** 3706–3722.

Wallace, J. M., G. H. Lim, and M. L. Blackmon, 1988: Relationship between cyclone tracks, anticyclone tracks, and baroclinic waveguides. *J. Atmos. Sci.,* **45,** 439–462.

Yang, G.-Y., and B. J. Hoskins, 1996: Propagation of Rossby waves of nonzero frequency. *J. Atmos. Sci.,* **53,** 2365–2378.

Zhang, X.-D., J. E. Walsh, J. Zhang, U. S. Bhatt, and M. Ikeda, 2004: Climatology and interannual variability of Arctic cyclone activity: 1948–2002. *J. Climate,* **17,** 2300–2317.